ACS OMEGA

http://pubs.acs.org/journal/acsodf

Article

Re-evaluation of the Fijianolide/Laulimalide Chemotype Suggests an Alternate Mechanism of Action for C-15/C-20 Analogs

Joseph D. Morris, Leila Takahashi-Ruiz, Lauren N. Persi, Jonathan C. Summers, Erin P. McCauley, Peter Y. W. Chan, Gabriella Amberchan, Itzel Lizama-Chamu, David A. Coppage, Phillip Crews, April L. Risinger,* and Tyler A. Johnson*

Cite This: *ACS Omega* 2022, 7, 8824−8832

Read Online

ACCESS | Metrics & More | Article Recommendations | Supporting Information

ABSTRACT: Herein, we report on naturally derived microtubule stabilizers with activity against triple negative breast cancer (TNBC) cell lines, including paclitaxel, fijianolide B/laulimalide (**3**), fijianolide B di-acetate (**4**), and two new semisynthetic analogs of **3**, which include fijianolide J (**5**) and fijianolide L (**6**). Similar to paclitaxel, compound **3** demonstrated classic microtubule stabilizing activity with potent (GI_{50} = 0.7−17 nM) antiproliferative efficacy among the five molecularly distinct TNBC cell lines. Alternatively, compounds **5** or **6**, generated from oxidation of C-20 or C-15 and C-20 respectively, resulted in a unique profile with reduced potency (GI_{50} = 4−9 μM), but improved efficacy in some lines, suggesting a distinct mechanism of action. The C-15, C-20 di-acetate, and dioxo modifications on **4** and **6** resulted in compounds devoid of classic microtubule stabilizing activity in biochemical assays. While **4** also had no detectable effect on cellular microtubules, **6** promoted a reorganization of the cytoskeleton resulting in an accumulation of microtubules at the cell periphery. Compound **5**, with a single C-20 oxo substitution, displayed a mixed phenotype, sharing properties of **3** and **6**. These results demonstrate the importance of the C-15/C-20 chiral centers, which appear to be required for the potent microtubule stabilizing activity of this chemotype and that oxidation of these sites promotes unanticipated cytoskeletal alterations that are distinct from classic microtubule stabilization, likely through a distinct mechanism of action.

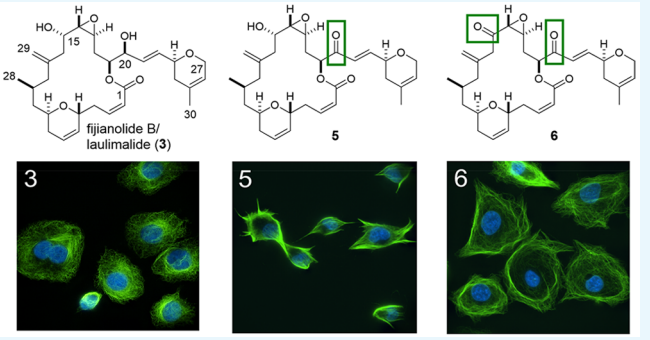

INTRODUCTION

Some of the most effective frontline chemotherapeutic agents for the treatment of triple negative breast cancers (TNBCs) are the taxane class of microtubule stabilizers, including paclitaxel.[1,2] Over the past decades, a number of other microtubule targeted agents (MTAs) derived from natural products have been developed for the treatment of breast cancer with a particular focus on therapeutics that have distinct binding sites as compared to the taxanes or the ability to circumvent clinically relevant forms of taxane resistance.[3] A noteworthy example includes Ixempra, an analog of the myxobacteria-derived epothilone B that binds within the taxane pocket and may have advantages in taxane-resistant settings.[4] Selected examples of marine-derived microtubule stabilizers that have undergone preclinical development include the covalent microtubule stabilizer zampanolide, which binds within the taxane pocket,[5] as well as peloruside A[6] and the fijianolides/laulimalides,[7−9] which jointly define a microtubule stabilizer binding site that is completely nonoverlapping with the taxanes.[8]

The fijianolide/laulimalide chemotype has received considerable attention over the past 20 years as a potent class of microtubule stabilizers that demonstrate activity against taxane-resistant cell lines, including multidrug resistant cells expressing the p-glycoprotein drug efflux pump.[8−10] Fijianolide A/isolaulimalide (**1**), neolaulimalide (**2**), and laulimalide/fijianolide B (**3**), shown in Figure 1, were independently characterized in 1988[11,12] and 1996.[13] While **1** was found to be modestly potent, **2** and **3** were recognized early on to impart considerable cytotoxic potency against a wide variety of cancer cell lines. A landmark discovery in 1999 revealed that the cytotoxic mechanism of action (MOA) of **3** against cancer cell lines was due in part to its ability to stabilize microtubules.[9] This was later confirmed for **2** as well in 2009.[13] Interestingly, the microtubule binding site for this chemotype was found to be on the microtubule exterior, distinct from the taxane site, enabling this structural class to retain potency against taxane-

Received: December 18, 2021
Accepted: February 23, 2022
Published: March 7, 2022

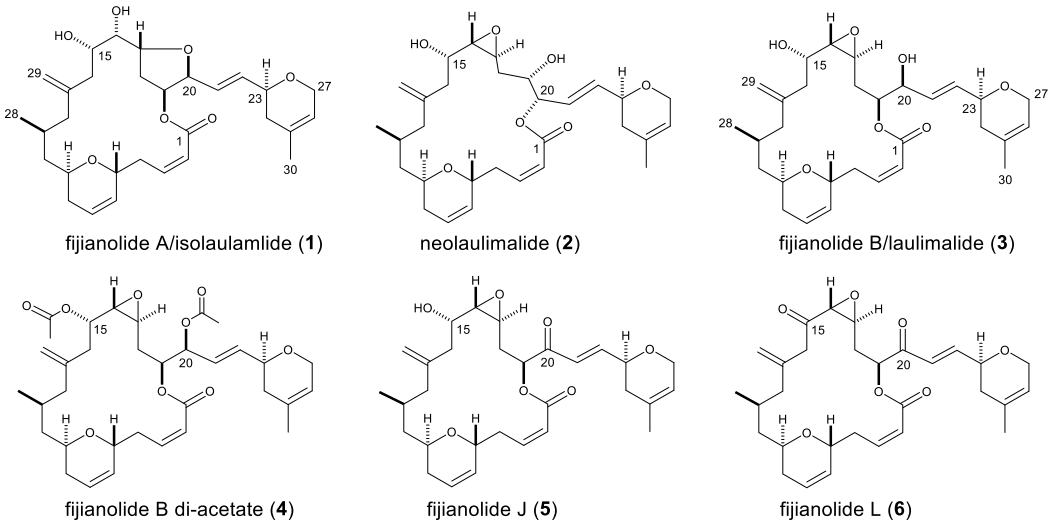

Figure 1. Structures of fijianolide A/isolaulimalide (**1**), neolaulimalide (**2**), fijianolide B/laulimalide (**3**), fijianolide B di-acetate (**4**), and fijianolides J (**5**) and L (**6**).

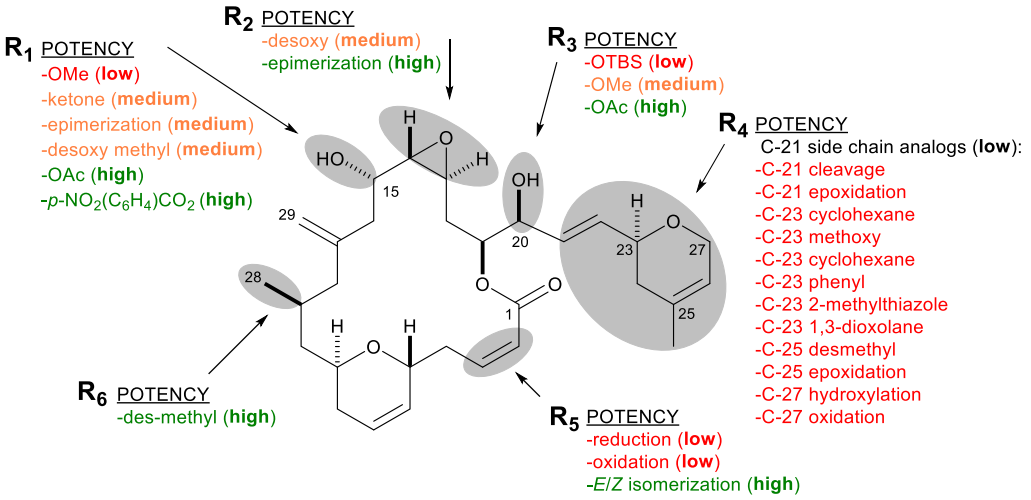

Figure 2. Summary of structure activity relationship (SAR) studies with **3** involving 28 modifications to R-groups (R_1–R_6), resulting in low (IC_{50} > 1000 nM, red), medium (IC_{50} = 100–1000 nM, orange), or high (IC_{50} < 100 nM, green) potency analogs (in parentheses) based on potency to selected cancer cell lines in Table S1.

resistant cell lines.[8−10] These findings have motivated 14 total syntheses of **3** by multiple research groups.[7,13−16] In vivo antitumor evaluations reported antitumor activity for **3** in HCT-116 xenografts[16] and a complete lack of efficacy in MDA-MB-435 and HT-1080 xenografts over a range of doses and schedules.[17] Alternatively, significant efforts have been made studying **3** for its use as a novel molecular probe to investigate microtubule dynamics because of its distinct binding motif with *β*-tubulin.[18−29]

Stability studies noted the more potent **3** isomerized to the less potent **1** by a potential S_N2 attack on C-17 of the epoxide by the C-20 hydroxyl group upon exposure to acidic conditions.[11,12] Isomerization of **2** to **1** was also observed, albeit over a much longer period of time (2 days) compared to that of **3** to **1** (2 h).[13] From these studies, it appears **2** undergoes a much slower conversion involving ring contraction to generate **3**, then isomerizes to **1**, rendering **2** to be more stable then **3**. However, further studies to pursue **2** as a therapeutic lead have been stymied because it has not been reliably isolated from natural sources, being only reported once.[13] These results highlighted the need to develop analogs of **3** with enhanced stability and retained potency to expand the understanding of the cytotoxic structure−activity relationship (SAR) of this chemotype.[15] To date, this has resulted in the generation of 37 distinct analogs of **3** summarized in Figure 2 and shown in Table S1.[8,11,13,15,16,30−35] Figure 2 depicts the relative impact of modifications to each of six different chemical regions of **3**, labeled as R_1–R_6, on potency to result in low (IC_{50} > 1000 nM), medium (IC_{50} = 100–1000 nM) or high (IC_{50} < 100 nM) potency analogs against a variety of cancer cell lines (individual IC_{50} values listed in Table S1). These data highlight the significant amount of medicinal chemistry that has been conducted with this chemotype by over a dozen different research groups to optimize the potency and stability of this structural class for therapeutic development. However, it is important to note most of these studies did not confirm whether the antiproliferative potency of these analogs was due to the same mechanism of microtubule stabilization as for **3**, which complicates the interpretation of these SAR studies.

https://doi.org/10.1021/acsomega.1c07146
ACS Omega 2022, 7, 8824−8832

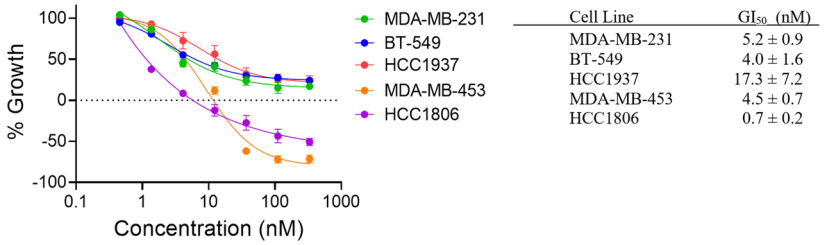

Figure 3. Antiproliferative and cytotoxic effects of **3** in a panel of molecularly diverse triple negative breast cancer (TNBC) cell lines. The cellular density at the time of compound addition is represented as the dashed line at $y = 0$, which allows for determination of the concentration that inhibits proliferation by 50% (y = 50) as the GI_{50} value. Cytotoxicity is evident from values that fall below the dashed line. Mean ± SEM, $n = 3$ independent experiments.

Table 1. Antiproliferative Potency of Paclitaxel and 3−6 Against Triple Negative Breast Cancer Cell Lines[a]

	GI_{50} (nM)		
compound	MDA-MB-231	HCC1806	BT-549
paclitaxel	3.3 ± 0.6	0.9 ± 0.3	2.8 ± 0.7
fijianolide B/laulimalide (**3**)	5.2 ± 0.9	0.7 ± 0.2	4.0 ± 1.6
fijianolide B di-acetate (**4**)	234 ± 104	110 ± 21	300 ± 25
fijianolide J (**5**)	4300 ± 700	4100 ± 800	5300 ± 800
fijianolide L (**6**)	8700 ± 1000	7900 ± 1000	6500 ± 500

[a]The concentration of each compound that inhibited the growth of each triple negative breast cancer (TNBC) cell line by 50% as compared to the time of drug addition (GI_{50}) was determined using the SRB assay. Mean ± SEM, $n = 3$−4 independent experiments

A key takeaway from Figure 2 is that structural variations to region R_4 resulted in a dozen new analogs, but all with potency in the micromolar range, indicating modifications to the C-21 to C-27 side chain region of this chemotype are not well tolerated. Structural variations to regions R_1−R_3 and R_5 had variable effects on potency depending on the specific modification. Selected examples of the potency in IC_{50} to cancer cell lines from analogs of **3** with modifications to regions R_1−R_3 are shown (in entries 2−8) in Table S1. A large OTBS ether modification at the C-20 hydroxyl drastically reduced potency (>1000 nM), whereas more minor methoxy and acetoxy modifications at this position were better tolerated with only moderately diminished potencies of 240 and 91 nM, respectively.[30,31] Similarly, a methoxy substitution on C-15 significantly reduces potency (>1000 nM), while an acetoxy modification on C-15 is well tolerated (23 nM). A di-acetate modification of both C-15 and C-20 (fijianolide B di-acetate, **4**[11]) also led to a moderate reduction in potency of 289 nM.[30] Epimerization of C-15 also produced a compound with moderately diminished potency (176 nM) although no mention of stability was reported.[30] Lastly, oxidation of C-15 to a ketone in combination with a reduction of the epoxide (desepoxide) completely abrogated activity, but it is unclear the effect of C-15 oxidation on its own. On the basis of these data and that **2** retained the potency of **3**, but with improved stability, we hypothesized that (a) targeted oxidation of the C-15 and C-20 stereocenters and (b) selected oxidation followed by reduction of C-20 to make the hydroxy epimer, could provide new lead compounds with retained nM potency, improved stability and ease of synthesis. Herein we describe the results of our hypothesis that include evaluations of **3**, as well as C-15 and C-20 modified analogs, against selected triple negative breast cancer (TNBC) cell lines, which led to the unanticipated identification of a novel mechanism of action independent of direct microtubule stabilization for this chemotype.

RESULTS AND DISCUSSION

Our first step was to evaluate the antiproliferative and cytotoxic effects of **3** in a panel of five molecularly diverse triple negative breast cancer (TNBC) cell lines taking into account the cellular density at the time of compound addition, which is represented by the dashed line at $y = 0$ in Figure 3. Consistent with published data in other cell lines, **3** demonstrated potent antiproliferative activity in each TNBC line with concentrations that inhibited growth by 50% (GI_{50}; $y = 50$ in Figure 3) ranging from 0.7 nM in the HCC1806 line to 17.3 nM in the HCC1937 cell line. In contrast, the efficacy of **3** varied among cell lines with cytotoxicity only observed in the MDA-MB-453 and HCC1806 cell lines as evidenced by decreased cellular density as compared to the time of compound addition (values dropping below the dashed line at $y = 0$). This is consistent with the relative efficacy of these cell lines to other classes of MTAs and demonstrates that **3** retains potent antiproliferative effects in TNBC models.

Next, we generated the known fijianolide B di-acetate (**4**)[10,30] by acetylating the hydroxyl groups on C-15 and C-20. This began with pure **3** to generate **4** by employing methods described previously in the Experimental Section.[11,30] As noted above, we hypothesized the stability of **3** could be improved, while also simplifying its total synthesis, by eliminating the C-15 and C-20 chiral centers. This involved oxidizing **3** at C-15 and C-20 using Dess−Martin periodinane (DMP) to produce the C-20 mono-oxo fijianolide J (**5**) along with the C-15, C-20 dioxo fijianolide L (**6**) as described in the Experimental Section. Using one molar equivalent of DMP with **3** led to the production of nearly pure **5**, while use of excess of 2 mol equiv DMP with **3** led to a mixture of **5** and **6**. Under no circumstances were we able to oxidize C-15 without oxidizing C-20 on **3** using DMP. Structural assignment of **4**−**6** was achieved by a combination of 1D and 2D NMR experiments and ESI-HAMS as shown in Tables S2 and S3 and Figures S2−S16. An additional C-15/C-20 dimethoxy analog of **3** (named fijianolide K) was also generated but not in sufficient quantity

https://doi.org/10.1021/acsomega.1c07146
ACS Omega 2022, 7, 8824−8832

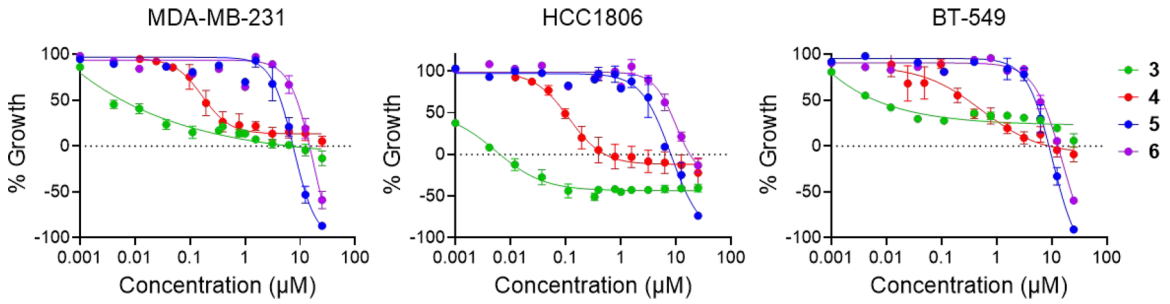

Figure 4. Concentration-dependent antiproliferative and cytotoxic effects of **3** (green), **4** (red), **5**, (blue), and **6** (purple) in triple negative breast cancer (TNBC) cell lines: (A) MDA-MB-231, (B) HCC1806, and (C) BT-549. The cellular density at the time of compound addition is represented as the dashed line at $y = 0$. Cytotoxicity is evident from values that fall below the dashed line (see arrows). Mean ± SEM, $n = 3–4$ independent experiments.

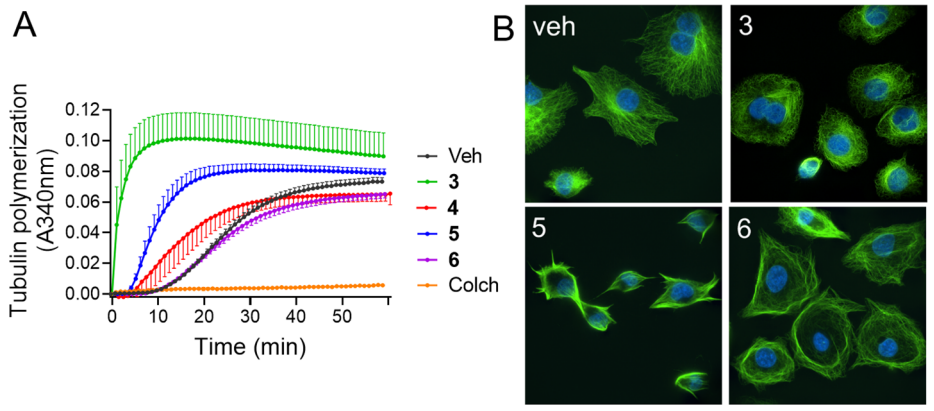

Figure 5. Fijianolides modified at C-15, C-20 have distinct effects on tubulin as compared to **3**. (A) Biochemical tubulin polymerization assay where 20 μM purified tubulin heterodimers are incubated in the presence of 20 μM of **3**–**6**. The microtubule destabilizer colchicine (colch) is used as a negative control. (B) Immunofluorescence of microtubules (green) and DNA (blue) in BT-549 cells treated for 8 h with vehicle (veh), 100 nM of **3**, or 20 μM of **5** and **6**. Data for compound **4** is not shown as it resembled the vehicle (veh) control.

to be fully structurally characterized and or evaluated in our biological assays.

We evaluated the potency and efficacy of **4**–**6** in a subset of TNBC cell lines. Consistent with previous reports in the MDA-MB-435 melanoma line,[30] we found that **4** had approximately 100-fold reduced potency as compared to **3** in our panel of TNBC lines in Table 1. Both compounds **5** and **6** had approximately 1000-fold reduced antiproliferative potency as compared to **3** in the MDA-MB-231, HCC1806, and BT-549 cell lines over 48 h as shown in Table 1. When we more closely interrogated the concentration-dependent response of these compounds on cellular growth and cytotoxicity, we observed that in spite of their decreased antiproliferative potency, compounds **5** and **6** actually had improved cytotoxic efficacy as compared to **3** or **4** at these higher μM concentrations, particularly in the MDA-MB-231 and BT-549 cell lines (Figure 4). This distinct pharmacological profile suggested that compounds **5** and **6** did not just have reduced potency, but that they likely had a distinct mechanism of action as compared to the parent compound **3**. To address this, we compared the ability of these compounds to polymerize microtubules both in biochemical preparations as well as in cells. We found that **5** had a reduced rate of biochemical tubulin polymerization as compared to **3** whereas neither **4** nor **6** were able to promote the polymerization of purified tubulin even when present at equimolar (20 μM) concentrations with tubulin heterodimers (Figure 5A).

We, further, evaluated the effects of these compounds on cellular microtubules in BT-549 cells. While **3** demonstrated classic cellular microtubule bundling, **4** had no effect on the cellular microtubule structure at concentrations up to 10 μM (data not shown). While compounds **5** and **6** did not promote classical microtubule stabilization in cells, they led to distinct phenotypes of short microtubule tufts for **5** or a roping of microtubules around the cellular periphery for **6** (Figure 5B). Importantly, these changes to the interphase microtubule cytoskeleton were observed 8 h after compound addition before any evidence of cytotoxicity was observed for **5** or **6**. Together, these data demonstrate that the dual C-15/C-20 acetylation or oxidation of **3** effectively eliminates direct microtubule stabilizing activity and reduces cellular potency. This reduced potency is associated with a distinct mechanism of action for compounds **5** and **6**, precluding this activity being due to trace amounts of the parent compound. Although, we cannot distinguish whether the micromolar potency observed with **4** is due to reduced activity of the modified compound or some degree of esterification of **4** into **3** in cells, co-sedimentation studies suggest that the activity of **4** is not likely due to contamination of the sample with small amounts of **3** (Figure S17). However, we cannot distinguish whether the micromolar potency observed with **4** is due to reduced activity of the modified compound, minor traces of **3**, or some degree of esterification of **4** into **3** in cells. Regardless, we conclude that either acetylation or oxidation of C-15/C-20 moieties on **3**

https://doi.org/10.1021/acsomega.1c07146
ACS Omega 2022, 7, 8824–8832

results in a loss of activity and, in the case of oxidation, results in compounds with a distinct mechanism of action.

Because of the complete lack of direct microtubule polymerization observed for **6** and the unique accumulation of cellular microtubules around the cell periphery, we further interrogated its cytoskeletal effects. Vimentin is a type III intermediate filament (IF) protein expressed in mesenchymal cells and is found in breast cancer cells that have undergone epithelial-to-mesenchymal transition (EMT), including BT-549 cells. We found that 8 h of treatment with **6** was sufficient to completely collapse vimentin to a perinuclear localization as shown in Figure 6A and shift the distribution of F-actin fibers

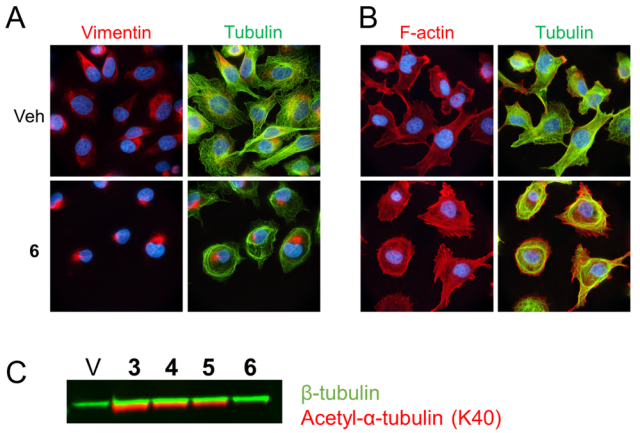

Figure 6. Cytoskeletal effects of **6**. (A) Immunofluorescence for vimentin (red) and DNA (blue) without (left panels) or with (right panels) microtubules (green) in BT-549 cells treated with vehicle or 20 μM **6** for 8 h. (B) Immunofluorescence for F-actin (red) and DNA (blue) without (left panels) or with (right panels) microtubules (green) in BT-549 cells treated with vehicle or 20 μM **6** for 8 h. (C) Immunoblot of total β-tubulin (green) or acetylated α-tubulin (K40) in BT-549 cells treated with vehicle, 100 nM **3**, or 20 μM indicated analogs for 8 h.

from the cell periphery to a more uniform distribution throughout the cell (Figure 6B). This collapse of the vimentin IF network to a perinuclear localization is strikingly similar to that induced by expression of the α-tubulin deacetylase, HDAC6, or a nonacetylatable variant of tubulin (K40R).[36] Indeed, **6** is distinct from the parent compound in that it is unable to promote the acetylation of α-tubulin, which has been previously reported for **3** (Figure 6C).[18] Importantly, this vimentin collapse is also associated with oncogene transformation and increased cellular stiffness, which is associated with increased invasion, suggesting that compounds that promote this phenotype would not be effective anticancer agents. Presumably, the changes in cellular microtubule structure are mediated through a maintained interaction of **6** with the microtubule exterior that does not increase protofilament stability, but instead leads to distinct changes to the microtubule and vimentin cytoskeleton. These data are consistent with reports by Mooberry et al, who saw a strikingly similar phenotype described as "long thick ropy microtubule structures" when cells were treated with an analog of **3** that was methylated at C-20 and lacked the C-16, C-17 epoxide, which also alters the orientation of C-15.[31] Intriguingly, neither of these individual modifications produced this phenotype, suggesting that a disruption at both of these moieties is necessary to shift the cytoskeletal mechanism of action of this compound. Our data are consistent in that they also show that the oxidation of C-20 alone is not sufficient for a full phenotypic shift, but rather that oxidation of both C-15 and C-20 is required to completely eliminate microtubule polymerizing activity and promote the distinct peripheral distribution of microtubules shown in Figures 5B and 6.

CONCLUSIONS

While the clinical future of the fijianolide/laulimalide chemotype as a monotherapy remains uncertain, its unique binding site provides synergistic activity in combination with taxane-site binding MTAs and allows it to circumvent some taxane-associated drug resistance mechanisms. In the current study, we hypothesized that the creation of a C-20 hydroxy epimer of **3** could serve as a viable new analog for the relatively unexplored SAR epimerization studies of this chemotype. However, our results demonstrate that the observed cytotoxicity for C-15/C-20 oxidized derivatives of **3** is due to a distinct mechanism of action as compared to the direct microtubule stabilizing activity of **3**. This is a valuable finding as it prompts the need to reinterpret SAR data reported for this compound class, particularly when the activity of an analog is reported only as an IC_{50} value with no follow up mechanistic evaluations to ensure that the SAR is on target for the microtubule stabilizing activity of the fijianolide/laulimalide chemotype. An additional advantage of these more detailed mechanistic evaluations is that they alleviate concerns that the reduced potency of an analog is due to contamination with trace amounts of the parent compound.

We propose that at least some of the inconsistency in the literature regarding the impact of modifications to fijianolide/laulimalide analogs, particularly at C-15/C-20, is due to the fact we demonstrate that substitutions at those sites can change the mechanism of the antiproliferative and cytotoxic effects of this compound class. Our findings more specifically demonstrate that the chiral centers of C-15/C-20 are critical for the microtubule stabilizing activity of **3** and that even minor modifications to these moieties, intended to improve compound stability, are incompatible with the direct microtubule stabilizing activity of this structural class. The finding that **6** can promote a distinct relocalization of cellular microtubules and other components of the cytoskeleton in the absence of direct microtubule stabilization or tubulin acetylation in cells suggests that this analog could retain the ability to interact with the fijianolide/laulimalide binding site on tubulin, but that the lack of chiral centers at C-15/20 leads to distinct allosteric effects downstream of its binding to alter its mechanism of action. Ultimately, our findings provide additional insight into the mechanistic importance of the C-15/C-20 moieties on the fijianolide/laulimalide chemotype and provide a cautionary tale of the importance of interrogating detailed mechanistic SAR data for this and other compound classes when undertaking these types of studies.

EXPERIMENTAL SECTION

General Experimental Procedures. NMR experiments were conducted on several different spectrometers that include (1) a Varian (Agilent) spectrometer fitted with a 5 mm triple-resonance probe (^{1}H, ^{13}C, ^{15}N) with 400 MHz resonance for ^{1}H experiments and 100 MHz resonance for ^{13}C experiments, (2) a Bruker Avance III HD spectrometer fitted with a 5 mm BBO smart probe with 500 MHz resonance for ^{1}H experiments

https://doi.org/10.1021/acsomega.1c07146
ACS Omega 2022, 7, 8824−8832

and 125 MHz for ^{13}C experiments, (3) a Varian (Agilent) Inova fitted with a 5 mm triple-resonance cryoprobe (^{1}H, ^{13}C, ^{15}N) with 600 MHz for ^{1}H experiments and 150 MHz for ^{13}C experiments, and (4) a Bruker AV fitted with a triple-resonance (^{1}H, ^{13}C, ^{15}N) cryoprobe with 700 MHz resonance for ^{1}H experiments and 175 MHz for ^{13}C experiments. LCMS and high accuracy mass spectrometer measurements were performed on a VelosPro Orbitrap mass spectrometer (Thermo Scientific) coupled to a photodiode array detector with the following experimental parameters: ion transfer tube temperature, 380 °C; vaporization temperature, 300 °C; sheath gas pressure, 60 psi; auxiliary gas flow, 20 abu; spray voltage, 3.0 kV; S-lens RF level, 68.3%.

Biological Material, Collection, and Identification. Specimens of the marine sponge *Cacospongia mycofijiensis* were obtained by scuba in Vanuatu as reported previously.[37,38] Taxonomic identification was based on comparison of characteristic biological features to other samples in the UC Santa Cruz sponge repository. Voucher specimens and underwater photos are available on request.

Extraction and Isolation. Extracts of *C. mycofijiensis* were processed according to previous reported methods.[39] Repository dichloromethane methanol extracts (coded DMM, not traditionally processed due to their high lipophilic content) were obtained from the UCSC marine sponge repository. The DMM extract was used in the repeated scale up HPLC isolation of **3**, for use in semisynthesis and further biological evaluation. HPLC purification was performed on a semi-preparative column (Phenomenex Inc. Luna© 5 μm C18(2) 100 Å 10 × 250 mm) in conjunction with a 4.0 × 3.0 mm C18 (octadecyl) guard column and cartridge (holder part number: KJ0−4282, cartridge part number: AJ0−4287, Phenomenex Inc., Torrance, CA, USA). A reversed-phased linear gradient was employed (30:70 CH_3CN/H_2O to 80:20 over 50 min, ramping up to 100% CH_3CN from 51 to 61 min, then returning to 30:70 for re-equilibration from minutes 62 to 73). Compound detection was measured with an Applied Biosystems 759a UV detector at a single wavelength λ_{max} = 230 nm. For the DMM extracts, four major HPLC fractions began to elute at approximately 46 min. For each HPLC sample of the DMM extracts ([15 mg/150 μL], MeOH), approximately 0.6 mg of compound **3**, 0.3 mg of zampanolide, 0.7 mg of latrunculin A, and 1.5 mg of mycothiazole were liberated. All purified compounds were dried under an N_2 stream, stored in an amber vial, and purged with gaseous argon then sealed in a dark desiccator under vacuum. Compound **4** was generated by semisynthesis according to previously reported methods.[11,30] A sample of **3** (4.35 mg) along with 1000 μL acetic anhydride and 1000 μL dry pyrdine were added to a reaction vial. The mixture was stirred for 24 h before the reaction was quenched with 1000 μL of d-H_2O and 1000 μL of dichloromethane (DCM). The layers were inverted and allowed to separate before the DCM layer was removed from the reaction vial and dried under an N_2 stream. The dried DCM layer was purified using RP-HPLC (Phenomenex Luna 5 μm C18(2) 100 Å 10 × 250 mm) to yield one major fraction determined to be compound **4** (3.43 mg, 68%). Compounds **5** and **6** were generated by semisynthesis. A sample of **3** (15.42 mg) and Dess−Martin periodinane (64 mg, 4.4 mol equiv) were added to 800 μL of dichloromethane.[40] The mixture was stirred for 22 h. The reaction mixture, along with 100 mL of water and 100 mL of hexanes, were added to a separatory funnel. The aqueous and organic layers were collected separately and the organic layer was dried under an N_2 stream. The dried crude organic layer (10.15 mg) was purified using RP-HPLC (Phenomenex Luna 5 μm C18(2) 100 Å 10 × 250 mm) to yield two major fractions determined to be compounds **5** (1.70 mg, 14%) and **6** (1.05 mg, 8%).

Cell Lines. MDA-MB-231, HCC1937, MDA-MB-453, and HCC1806 human TNBC cell lines were received from ATCC. BT-549 cells were obtained from the Georgetown University Lombardi Comprehensive Cancer Center, Washington, DC. BT-549, HCC1806 and HCC1937 cells were grown in RPMI 1640 medium (Gibco) supplemented with up to 10% FBS (Corning). MDA-MB-231 and MDA-MB-453 were cultured in modified IMEM supplemented with L-glutamine and up to 10% FBS. Cell line identity was authenticated by STR-based profiling (Genetica DNA Laboratories). All cells were grown at 37 °C and 5% CO_2 in an incubator and routinely tested for mycoplasma contamination.

Antiproliferative and Cytotoxic Assay. TNBC cells were seeded into a 96-well plate and, after adhering overnight, were treated with vehicle alone or compounds at concentrations from 1 nM to 20 μM in a final volume of 0.5% EtOH vehicle for 48 h. A separate plate was fixed with 10% TCA at the time of drug addition to provide a readout of cellular density, which was used to differentiate antiproliferative from cytotoxic effects. 48 h after treatment, cells were fixed with 10% TCA, and the protein stained with sulforhodamine B dye, which allowed for quantification of cellular density proportional to absorbance at 560 nm using a Spectramax plate reader running SoftMax Pro 5.4 (Molecular Devices). The percent growth at each concentration was calculated using the equation [(48 h drug − time 0)/(48 h vehicle − time 0)]*100 and percent cytotoxicity as 100 − [(48 h drug/time 0)*100], where time 0 is the density of cells at the time of drug addition. Concentration-dependent antiproliferative effects were graphed using Graphpad (Prism) with error bars representing SEM as compared to the density at the time of drug addition as $y = 0$, the density of vehicle treated cells as $y = 100$, and a blank well as $y = -100$. Concentrations that caused a 50% inhibition of cell growth (GI_{50}, $y = 50$) were determined by nonlinear regression analysis of the data and are from 3 independent experiments each run in triplicate ± SEM.

Immunofluorescence. BT-549 cells were plated on glass coverslips treated with the indicated concentration of each compound or EtOH vehicle control for 8 h and then fixed with ice cold methanol for 5 min. Indirect immunofluorescence was used to detect β-tubulin (Sigma T-4026T) and nuclei stained with DAPI. Images were acquired on a Nikon widefield florescence microscope running NIS elements with multiple *z*-stacks.

Biochemical Tubulin Polymerization. The polymerization of purified porcine tubulin (Cytoskeleton; T240) was performed in GPEM buffer (80 mM PIPES pH 6.9, 2 mM MgCl2, 0.5 mM EGTA, and 1 mM GTP) in 10% glycerol. All components were kept on ice during preparation. Compounds (1 μL of 2 mM stocks) were added to individual wells of a 96-well plate in 100 μL of GPEM buffer with 20 μM tubulin to give equimolar concentrations of tubulin and drug. Microtubule polymerization was monitored at 37 °C by measuring the change in absorbance at 340 nm every minute for an hour using a SoftMax Pro 5.4 plate reader (Molecular Devices).

Immunoblotting. BT-549 cells were seeded in a 6-well dish and treated with ethanol (vehicle), 100 nM of **3**, or 20 μM of compounds **4**, **5**, or **6**. Cells were harvested by scraping and

https://doi.org/10.1021/acsomega.1c07146
ACS Omega 2022, 7, 8824−8832

lysed in 50 mM Tris, 1% IGEPAL CA-630, and 150 mM sodium chloride with protease inhibitor cocktail (Sigma-Aldrich), 10 mM sodium fluoride, 1 mM phenylmethylsulfonyl fluoride, and 200 μM sodium orthovanadate. Equal amounts of protein were loaded onto a Bolt 10% Bis−Tris Plus gel (Invitrogen) and transferred onto a PVDF Immobilon-FL membrane (Millipore). The membrane was blocked for 1 h at room temperature in 5% nonfat milk in TBST after which protein levels were evaluated by immunoblotting. Primary antibodies used were acetylated-α-tubulin (rabbit monoclonal antibody, 1:1000, 5335S, Cell Signaling Technologies) and total β-tubulin (mouse monoclonal antibody, 1:1000, T4026, Sigma-Aldrich). Secondary antibodies used were IRDye 800CW Goat antirabbit for acetylated α-tubulin (red) and 680CW goat antimouse for total β-tubulin (green) (1:5000 dilution, LI-COR Biosciences). The immunoblot was visualized using a LI-COR Biosciences Odyssey Fc Imager for 10 min at the 700CW channel and 2 min at the 800CW channel. Revert total protein staining confirmed equal loading of protein in each lane.

Paclitaxel. Obtained from Sigma-Aldrich. (T1912).

*Fijianolide B/Laulimalide (**3**).* White powder; ^{1}H and ^{13}C NMR data (C_6D_6) see Table S2 and Figure S1, consistent with previous reports,[16] ESI-HAMS m/z 515.2969 $[M + H]^+$ (calcd for $C_{30}H_{43}O_7$, 515.3009).

*Fijianolide B Di-acetate (**4**).* White powder; ^{1}H NMR data (C_6D_6) see Table S3 and Figure S2; LRMS m/z (599 $[M + H]^+$) (calcd for $C_{34}H_{47}O_9$).

*Fijianolide J (**5**).* White powder; ^{1}H and ^{13}C NMR data (C_6D_6) see Table S4 and Figures S3−S8; ESI-HAMS m/z (513.2728 $[M + H]^+$) (calcd for $C_{30}H_{41}O_7$, 513.2852).

*Fijianolide L (**6**).* White powder; ^{1}H and ^{13}C NMR data (C_6D_6) see Table S5 and Figures S9−S13; ESI-HAMS m/z (511.2574 $[M + H]^+$) (calcd for $C_{30}H_{39}O_7$, 511.2696).

■ ASSOCIATED CONTENT

Supporting Information

The Supporting Information is available free of charge at https://pubs.acs.org/doi/10.1021/acsomega.1c07146.

A summary of the structure activity relationship (SAR) data for published fijianolide B/laulimalide (**3**) analogs, NMR data of **3**−**6** with ^{1}H, ^{13}C, DEPT, gCOSY, HSQC, and HMBC data provided for **4**−**6**, and ESI-HAMS spectra for **3** and **5**−**6** (PDF)

■ AUTHOR INFORMATION

Corresponding Authors

April L. Risinger − *Department of Pharmacology, University of Texas Health Science Center at San Antonio, San Antonio, Texas 78229, United States;* orcid.org/0000-0002-4363-3268; Phone: (210) 567-6267; Email: risingera@uthscsa.edu

Tyler A. Johnson − *Department of Natural Sciences, Dominican University of California, San Rafael, California 94901, United States; Department of Chemistry & Biochemistry, University of California, Santa Cruz, California 95064, United States;* orcid.org/0000-0001-6816-726X; Phone: (415) 482-1983; Email: tyler.johnson@dominican.edu

Authors

Joseph D. Morris − *Department of Natural Sciences, Dominican University of California, San Rafael, California 94901, United States;* orcid.org/0000-0001-5218-425X

Leila Takahashi-Ruiz − *Department of Pharmacology, University of Texas Health Science Center at San Antonio, San Antonio, Texas 78229, United States*

Lauren N. Persi − *Department of Natural Sciences, Dominican University of California, San Rafael, California 94901, United States*

Jonathan C. Summers − *Department of Natural Sciences, Dominican University of California, San Rafael, California 94901, United States*

Erin P. McCauley − *Department of Chemistry & Biochemistry, University of California, Santa Cruz, California 95064, United States;* Present Address: Department of Chemistry and Biochemistry, California State University Dominguez Hills, Carson, CA, 90747, USA

Peter Y. W. Chan − *Department of Pharmacology, University of Texas Health Science Center at San Antonio, San Antonio, Texas 78229, United States;* orcid.org/0000-0002-3498-6301

Gabriella Amberchan − *Department of Chemistry & Biochemistry, University of California, Santa Cruz, California 95064, United States;* orcid.org/0000-0001-7923-8385

Itzel Lizama-Chamu − *Department of Chemistry & Biochemistry, University of California, Santa Cruz, California 95064, United States*

David A. Coppage − *Department of Chemistry & Biochemistry, University of California, Santa Cruz, California 95064, United States*

Phillip Crews − *Department of Chemistry & Biochemistry, University of California, Santa Cruz, California 95064, United States;* orcid.org/0000-0002-9061-9549

Complete contact information is available at: https://pubs.acs.org/10.1021/acsomega.1c07146

Author Contributions

A.L.R., and T.A.J. conceived the project. J.D.M. isolated compounds, designed and conducted synthesis experiments to generate analogs of **3**, and performed structure elucidation on synthetic analogs. L.N.P. and J.C.S. purified compounds and synthesized analogs of **3**. L.T.R., P.Y.W.C., and A.L.R. conducted bioassay studies. E.P.M., G.A., and I.L.C. conducted mass spectrometry experiments. D.A.C. analyzed SAR data of published analogs. J.D.M., P.C., A.L.R., and T.A.J. wrote the manuscript. All authors have given approval to the final version of the manuscript.

Notes

The authors declare no competing financial interest.

■ ACKNOWLEDGMENTS

We are grateful to Drs. Hasan Celik, Alicia Lund (UC Berkeley), and Jack Lee (UC Santa Cruz) for assistance with NMR experiments. Financial support was provided by NIH Grant R01 CA 47135 (P.C.), NIH Instrument Grant S10OD024998 (H. Celik), and the Voelcker Fund (A.R.). Additional financial support was provided by the American Society of Pharmacognosy (ASP) research starter grant (T.A.J.), Dominican University of California Summer Research

Grants (J.D.M., L.N.P., C.V.C., N.L.M., T.A.J.), and by the Fletcher Jones Endowment Fund of Dominican University of California (T.A.J.)

REFERENCES

(1) Harbeck, N.; Gnant, M. Breast Cancer. *Lancet* **2017**, *389*, 1134−1150.
(2) Zhou, J.; Giannakakou, P. Targeting Microtubules for Cancer Chemotherapy. *Curr. Med. Chem. − Anti-Cancer Agents* **2005**, *5*, 65−71.
(3) La Regina, G.; Coluccia, A.; Naccarato, V.; Silvestri, R. Towards Modern Anticancer Agents that Interact with Tubulin. *Eur. J. Pharm. Sci.* **2019**, *131*, 58−68.
(4) Khrapunovich-Baine, M.; Menon, V.; Yang, C.-P. H.; Northcote, P. T.; Miller, J. H.; Angeletti, R. H.; Fiser, A.; Horwitz, S. B.; Xiao, H. Hallmarks of Molecular Action of Microtubule Stabilizing Agents. Effects of Epothilone B, Ixabepilone, Peloruside A and Laulimalide on Microtubule Conformation. *J. Biol. Chem.* **2011**, *286* (13), 11765−11778.
(5) Field, J. J.; Pera, B.; Calvo, E.; Canales, A.; Zurwerra, D.; Trigili, C.; Rodríguez-Salarichs, J.; Matesanz, R.; Kanakkanthara, A.; Wakefield, S. J.; Singh, A. J.; Jiménez-Barbero, J.; Northcote, P.; Miller, J. H.; López, J. A.; Hamel, E.; Barasoain, I.; Altmann, K. H.; Díaz, J. F. Zampanolide, a potent new microtubule-stabilizing agent, covalently reacts with the taxane luminal site in tubulin α,β-heterodimers and microtubules. *Chem. Biol.* **2012**, *19*, 686−698.
(6) Gaitanos, T. N.; Buey, R. M.; Díaz, J. F.; Northcote, P. T.; Teesdale-Spittle, P.; Andreu, J. M.; Miller, J. H. Peloruside A does not bind to the taxoid site on beta-tubulin and retains its activity in multidrug-resistant cell lines. *Cancer Res.* **2004**, *64*, 5063−5067.
(7) Mulzer, J.; Ohler, E. Microtubule-stabilizing marine metabolite laulimalide and its derivatives: Synthetic approaches and antitumor activity. *Chem. Rev.* **2003**, *103*, 3753−3786.
(8) Pryor, D. E.; O'Brate, A.; Bilcer, G.; Diaz, J. F.; Wang, Y.; Wang, Y.; Kabaki, M.; Jung, M. K.; Andreu, J. M.; Ghosh, A. K.; Giannakakou, P.; Hamel, E. The microtubule stabilizing agent laulimalide does not bind in the taxoid site, kills cells resistant to paclitaxel and epothilones, and may not require its epoxide moiety for activity. *Biochemistry* **2002**, *41*, 9109−9115.
(9) Mooberry, S. L.; Tien, G.; Hernandez, A. H.; Plubrukarn, A.; Davidson, B. S. Laulimalide and isolaulimalide, new paclitaxel-like microtubule stabilizing agents. *Cancer Res.* **1999**, *59*, 653−660.
(10) Bennett, M. J.; Barakat, K.; Huzil, J. T.; Tuszynski, J.; Schriemer, D. C. Discovery and Characterization of the Laulimalide-Microtubule Binding Mode by Mass Shift Perturbation Mapping. *Cell Chem. Biol.* **2010**, *17*, 725−734.
(11) Quinoa, E.; Kakou, Y.; Crews, P. Fijianolides, polyketide heterocycles from a marine sponge. *J. Org. Chem.* **1988**, *53*, 3642−3644.
(12) Corley, D. G.; Herb, R.; Moore, R. E.; Scheuer, P. J.; Paul, V. J. Laulimalides: New potent cytotoxic macrolides from a marine sponge and a nudibranch predator. *J. Org. Chem.* **1988**, *53*, 3644−3646.
(13) Gollner, A.; Altmann, K. H.; Gertsch, J.; Mulzer, J. The Laulimalide Family: Total Synthesis and Biological Evaluation of Neolaulimalide, Isolaulimalide, Laulimalide and a Nonnatural Analogue. *Chem. - Eur. J.* **2009**, *15*, 5979−5997.
(14) Trost, B. M.; Amans, D.; Seganish, W. M.; Chung, C. K. Evaluating Transition-Metal-Catalyzed Transformations for the Synthesis of Laulimalide. *J. Am. Chem. Soc.* **2009**, *131*, 17087−17089.
(15) Trost, B. M.; Amans, D.; Seganish, W. M.; Chung, C. K. Total Synthesis of Laulimalide: Assembly of the Fragments and Completion of the Synthesis of the Natural Product and a Potent Analogue. *Chem. - Eur. J.* **2012**, *18*, 2961−2971.
(16) Johnson, T. A.; Tenney, K.; Cichewicz, R. H.; Morinaka, B. I.; White, K. N.; Amagata, T.; Subramanian, B.; Media, J.; Mooberry, S. L.; Valeriote, F. A.; Crews, P. Sponge-Derived Fijianolide Polyketide Class: Further Evaluation of Their Structural and Cytotoxicity Properties. *J. Med. Chem.* **2007**, *50*, 3795−3803.
(17) Liu, J.; Towle, M. J.; Cheng, H.; Saxton, P.; Reardon, C.; Wu, J.; Murphy, E. A.; Kuznetsov, G.; Johannes, C. W.; Tremblay, M. R.; Zhao, H.; Pesant, M.; Fang, F. G.; Vermeulen, M. W.; Gallagher, B. M., Jr.; Littlefield, B. A. In vitro and in vivo anticancer activities of synthetic (−)-laulimalide, a marine natural product microtubule stabilizing agent. *Anticancer Res.* **2007**, *27*, 1509−1518.
(18) Bennett, M. J.; Chan, G. K.; Rattner, J. B.; Schriemer, D. C. Low-dose laulimalide represents a novel molecular probe for investigating microtubule organization. *Cell Cycle* **2012**, *11*, 3045−3054.
(19) Das, V.; Sim, D. A.; Miller, J. H. Effect of taxoid and nontaxoid site microtubule-stabilizing agents on axonal transport of mitochondria in untransfected and ECFP-htau40-transfected rat cortical neurons in culture. *J. Neurosci. Res.* **2014**, *92*, 1155−1166.
(20) Das, V.; Miller, J. H. Non-taxoid site microtubule-stabilizing drugs work independently of tau overexpression in mouse N2a neuroblastoma cells. *Brain Res.* **2012**, *1498*, 121−132.
(21) Gajewski, M. M.; Alisaraie, L.; Tuszynski, J. A. Peloruside, Laulimalide, and Noscapine Interactions with Beta-Tubulin. *Pharm. Res.* **2012**, *29*, 2985−2993.
(22) Rey, M.; Sarpe, V.; Burns, K. M.; Buse, J.; Baker, C. A. H.; van Dijk, M.; Wordeman, L.; Bonvin, A. M. M. J.; Schriemer, D. C. Mass Spec Studio for Integrative Structural Biology. *Structure* **2014**, *22*, 1538−1548.
(23) Churchill, C. D. M.; Klobukowski, M.; Tuszynski, J. A. The Unique Binding Mode of Laulimalide to Two Tubulin Protofilaments. *Chem. Biol. Drug Des.* **2015**, *86*, 190−199.
(24) Prota, A. E.; Bargsten, K.; Northcote, P. T.; Marsh, M.; Altmann, K. H.; Miller, J. H.; Díaz, J. F.; Steinmetz, M. O. Structural Basis of Microtubule Stabilization by Laulimalide and Peloruside A. *Angew. Chem., Int. Ed.* **2014**, *53*, 1621−1625.
(25) Kanakkanthara, A.; Rowe, M. R.; Field, J. J.; Northcote, P. T.; Teesdale-Spittle, P. H.; Miller, J. H. βI-tubulin mutations in the laulimalide/peloruside binding site mediate drug sensitivity by altering drug-tubulin interactions and microtubule stability. *Cancer Lett.* **2015**, *365*, 251−260.
(26) Churchill, C. D.; Klobukowski, M.; Tuszynski, J. A. Analysis of the Binding Mode of Laulimalide to Microtubules: Establishing a Laulimalide-Tubulin Pharmacophore. *J. Biomol. Struct. Dyn.* **2016**, *34*, 1455−1469.
(27) Zúñiga, M. A.; Alderete, J. B.; Jaña, G. A.; Jiménez, V. A. Structural insight into the role of Gln293Met mutation on the Peloruside A/Laulimalide association with $\alpha\beta$-tubulin from molecular dynamics simulations, binding free energy calculations and weak interactions analysis. *J. Comput. Aided Mol. Des.* **2017**, *31*, 643−652.
(28) Castro-Alvarez, A.; Pineda, O.; Vilarrasa, J. Further Insight into the Interactions of the Cytotoxic Macrolides Laulimalide and Peloruside A with Their Common Binding Site. *ACS Omega* **2018**, *3*, 1770−1782.
(29) Zúñiga, M. A.; Alderete, J. B.; Jaña, G. A.; Fernandez, P. A.; Ramos, M. J.; Jiménez, V. A. Modulation of Lateral and Longitudinal Interdimeric Interactions in Microtubule Models by Laulimalide and Peloruside A Association: A Molecular Modeling Approach on the Mechanism of Microtubule Stabilizing Agents. *Chem. Biol. Drug Des.* **2018**, *91*, 1042−1055.
(30) Gallagher, B. M.; Fang, F. G.; Johannes, C. W.; Pesant, M.; Tremblay, M. R.; Zhao, H. J.; Akasaka, K.; Li, X. Y.; Liu, J. K.; Littlefield, B. A. Synthesis and biological evaluation of (−)-laulimalide analogues. *Bioorg. Med. Chem. Lett.* **2004**, *14*, 575−579.
(31) Mooberry, S. L.; Randall-Hlubek, D. A.; Leal, R. M.; Hegde, S. G.; Hubbard, R. D.; Zhang, L.; Wender, P. A. Microtubule-stabilizing agents based on designed laulimalide analogues. *Proc. Natl. Acad. Sci. U. S. A.* **2004**, *101*, 8803−8808.
(32) Wender, P. A.; Hegde, S. G.; Hubbard, R. D.; Zhang, L.; Mooberry, S. L. Synthesis and biological evaluation of (−)-laulimalide analogues. *Org. Lett.* **2003**, *5*, 3507−3509.
(33) Paterson, I.; Menche, D.; Hakansson, A. E.; Longstaff, A.; Wong, D.; Barasoain, I.; Buey, R. M.; Diaz, J. F. Design, synthesis and biological evaluation of novel, simplified analogues of laulimalide:

https://doi.org/10.1021/acsomega.1c07146
ACS Omega 2022, 7, 8824−8832

Modification of the side chain. *Bioorg. Med. Chem. Lett.* **2005**, *15*, 2243−2247.
(34) Wender, P. A.; Hilinski, M. K.; Skaanderup, P. R.; Soldermann, N. G.; Mooberry, S. L. Pharmacophore mapping in the laulimalide series: Total synthesis of a vinylogue for a late-stage metathesis diversification strategy. *Org. Lett.* **2006**, *8*, 4105−4108.
(35) Mooberry, S. L.; Hilinski, M. K.; Clark, E. A.; Wender, P. A. Function-oriented synthesis: biological evaluation of laulimalide analogues derived from a last step cross metathesis diversification strategy. *Mol. Pharmacol.* **2008**, *5*, 829−838.
(36) Rathje, L. Z.; Nordgren, N.; Pettersson, T.; Rönnlund, D.; Widengren, J.; Aspenström, P.; Gad, A. K. B. Oncogenes induce a vimentin filament collapse mediated by HDAC6 that is linked to cell stiffness. *Proc. Natl. Acad. Sci. U. S. A.* **2014**, *111* (4), 1515−1520.
(37) Morgan, J. B.; Mahdi, F.; Liu, Y.; Coothankandaswamy, V.; Jekabsons, M. B.; Johnson, T. A.; Sashidhara, K. V.; Crews, P.; Nagle, D. G.; Zhou, Y. D. The marine sponge metabolite mycothiazole: a novel prototype mitochondrial complex I inhibitor. *Bioorg. Med. Chem.* **2010**, *18*, 5988−5994.
(38) Sonnenschein, R. N.; Johnson, T. A.; Tenney, K.; Valeriote, F. A.; Crews, P. A Reassignment of (−)-Mycothiazole and the Isolation of a Related Diol. *J. Nat. Prod.* **2006**, *69*, 145−147.
(39) Thale, Z.; Johnson, T. A.; Tenney, K.; Wenzel, P. J.; Lobkovsky, E.; Clardy, J.; Media, J.; Pietraszkiewicz, H.; Valeriote, F. A.; Crews, P. Structures and cytotoxic properties of sponge-derived bisannulated acridines. *J. Org. Chem.* **2002**, *67*, 9384−9391.
(40) Johnson, T. A.; Morris, J. D.; Coppage, D. A.; Cook, C. V.; Persi, L. N.; Ogarrio, M. A.; Garcia, T. C.; McIntosh, N. L.; McCauley, E. P.; Media, J.; Maheshwari, M.; Valeriote, F. A.; Shaw, J.; Crews, P. Reinvestigation of Mycothiazole Reveals the Penta-2,4-dien-1-ol Residue Imparts Picomolar Potency and 8*S* Configuration. *ACS Med. Chem. Lett.* **2020**, *11*, 108−113.

https://doi.org/10.1021/acsomega.1c07146
ACS Omega 2022, 7, 8824−8832